The structural characterisation and elucidation of the electronic structure of the mononuclear Pt(III) complex $[Pt([9]aneS_3)_2]^{3+}$ ([9]aneS$_3$ = 1,4,7-trithiacyclononane)†

Emma Stephen, Alexander J. Blake, E. Stephen Davies, Jonathan McMaster* and Martin Schröder*

Received (in Cambridge, UK) 8th July 2008, Accepted 13th August 2008
First published as an Advance Article on the web 30th September 2008
DOI: 10.1039/b811645h

The mononuclear Pt(III) complex, $[Pt([9]aneS_3)_2]^{3+}$, has been isolated and characterised by X-ray crystallography; its electronic structure determined by EPR spectroscopy and DFT calculations.

Complexes incorporating a formal Pt(III) centre are rare and are dominated by reports of Pt(III)–Pt(III) or Pt(II)–Pt(III) dimers.[1–3] These dimers contain Pt centres bound by ligands such as $C_6F_5^-$ [1] and 2-hydroxypyridinate,[2,3] or Pt centres bound by direct metal–metal bonds as in $[Pt_2Cl_6\{HN{=}C(OH)C(CH_3)_3\}_4]$[4] and $[Pt_2(\mu\text{-}PPh_2)_2(C_6F_5)_4]$.[5] Square planar mononuclear Pt(III) complexes include $[Pt(C_6Cl_5)_4]^-$,[6] $[Pt(mnt)]^-$ [7,8] (mnt = maleodinitrile-dithiolato) and $Pt[(dcbdt)_2]^-$ [9] (dcbdt = dicyanobenzodithiolato), the electronic structures of which are extensively delocalised across the ligands. Noticeably absent from the literature is a fully characterised six co-ordinate mononuclear Pt(III) complex.

As part of our on-going studies of complexes containing unusual metal oxidation states,[10] we were interested in defining the extent to which homoleptic S_6 thioether co-ordination stabilises Pt(III). We report herein the structural and electronic properties of the first six co-ordinate Pt(III) complex, $[Pt([9]aneS_3)_2](PF_6)_3$ ([9]aneS$_3$ = 1,4,7-trithiacyclononane). While $[Pt([9]aneS_3)_2]^{3+}$ has been implicated in electron transfer studies involving $[Pt([9]aneS_3)_2]^{2+}$ in aqueous and MeCN solutions,[11] this species has not been isolated in the solid state previously nor characterised comprehensively.

Diamagnetic $[Pt([9]aneS_3)_2](PF_6)_2$ (**1**) was prepared by the reaction of [9]aneS$_3$ with $PtCl_2$ in H_2O–CH_3OH and an excess of NH_4PF_6. A single crystal of $[Pt([9]aneS_3)_2](PF_6)_2{\cdot}2MeCN$ (**1**·2MeCN) was obtained by diffusion of Et_2O into a solution of the complex in MeCN at room temperature. The crystal structure (Fig. S1 in ESI†) reveals an approximate square planar arrangement around the Pt(II) centre with Pt–S(4) = 2.2925(10), Pt–S(7) = 2.2995(10) Å and Pt···S(1) = 3.057(6) Å, S(4)–Pt–S(7) = 89.20(4)°.

The cyclic voltammogram of **1** in MeCN containing 0.2 M NBu_4PF_6 at a scan rate of 100 mV s^{-1} (Fig. S2 in ESI†) shows an oxidative process at E_p^a = +0.37 V *vs.* Fc^+/Fc at 298 K and a corresponding reduction at E_p^c = +0.22 V (ΔE = 142 mV). Oxidation of the complex at +0.6 V *vs.* Fc^+/Fc results in the formation of a colorless solution that was EPR-silent at room temperature and at 77 K. Coulometry confirms that the oxidation of **1** at E_p^a = +0.37 V is an overall two-electron process. These results are consistent with the formation of a Pt(IV) species, and UV/Vis spectroelectrochemistry using an optically transparent electrochemical (OTE) cell confirmed that this oxidation process is chemically reversible at 243 K and progresses *via* the formation of an intermediate species (Fig. 1). This intermediate is characterised by the emergence of a unique band at 396 nm (ε = 5700 M^{-1} cm^{-1}) that develops early on in the oxidation then diminishes in intensity as the electrolysis progresses. This band is not present in the UV/Vis spectrum of the fully oxidised species. The electrochemical oxidation of **1** in MeCN by one electron yielded an intensely yellow coloured EPR-active solution, consistent with the formation of $[Pt([9]aneS_3)_2](PF_6)_3$ (**2**).

Single crystals of $[Pt([9]aneS_3)_2](PF_6)_3{\cdot}MeCN$ (**2**·MeCN) (Fig. 2) were grown as dark yellow plates by vapour diffusion of Et_2O into a solution of **2** generated by the one-electron oxidation state of **1** in MeCN containing 0.1 M NBu_4PF_6. The X-ray crystal structure shows a distorted octahedral stereochemistry at the Pt centre. The asymmetric unit contains one $[Pt([9]aneS_3)_2]^{3+}$ cation, three PF_6^- anions and one MeCN

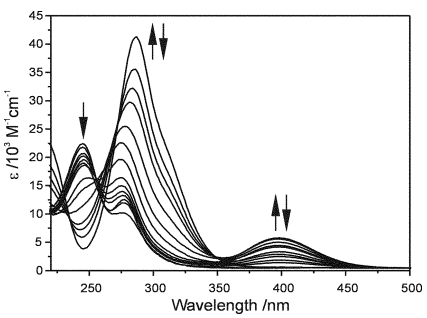

Fig. 1 *In situ* UV/Vis absorption spectrum of $[Pt([9]aneS_3)_2](PF_6)_2$ in MeCN (0.2 M NBu_4PF_6, 243 K) upon oxidation at +0.69 V (*vs.* Fc^+/Fc).

The School of Chemistry, The University of Nottingham, University Park, Nottingham, UK NG7 2RD.
E-mail: M.Schroder@nottingham.ac.uk.
E-mail: j.mcmaster@nottingham.ac.uk;
Fax: +44 115 951 3563; Tel: +44 115 951 3490

† Electronic supplementary information (ESI) available: Crystallographic data for $[Pt([9]aneS_3)_2](PF_6)_2$ and $[Pt([9]aneS_3)_2](PF_6)_3$, experimental preparations for $[Pt([9]aneS_3)_2](PF_6)_2$ and $[Pt([9]aneS_3)_2](PF_6)_3$, electrochemistry, EPR simulations and DFT calculations. CCDC 694378 and 694379. For ESI and crystallographic data in CIF or other electronic format, see DOI: 10.1039/b811645h

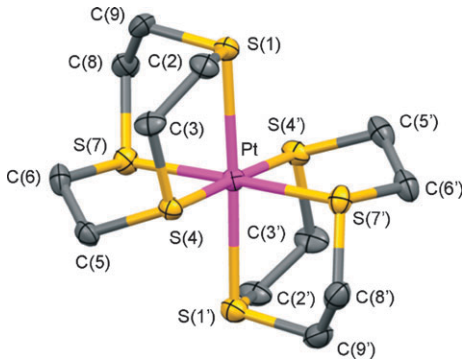

Fig. 2 A view of the $[Pt([9]aneS_3)_2]^{3+}$ cation in **2**·MeCN; displacement ellipsoids are drawn at the 50% probability level and hydrogen atoms are omitted for clarity.

solvent molecule. The Pt centre is bound by six S-donors from two ligands in a distorted octahedron. The Pt–S distances [Pt–S(1) = 2.5832(14), Pt–S(1′) = 2.5762(13), Pt–S(4) = 2.3467(15), Pt–S(4′) = 2.3445(14), Pt–S(7) = 2.3423(13), Pt–S(7′) = 2.3442(14) Å] and bond angles [S(1′)–Pt–S(1) = 177.62(6), S(4′)–Pt–S(4) = 178.88(6), S(7′)–Pt–S(7) = 178.70(5), S(4′)–Pt–S(1) = 94.04(5), S(7′)–Pt–S(1) = 93.41(5), S(4)–Pt–S(1) = 87.08(5), S(7)–Pt–S(1) = 87.88(5)°] show an overall axial compression of the co-ordination sphere compared to that of $[Pt([9]aneS_3)_2]^{2+}$ in **1**·2MeCN. Thus, going from Pt(II) to Pt(III) results in a shortening of the axial Pt–S interactions and an elongation of the Pt–S equatorial bonds consistent with a Jahn–Teller distorted d^7 Pt(III) centre.

The frozen solution X-band EPR spectrum of $[Pt([9]aneS_3)_2]^{3+}$, prepared electrochemically or by chemical oxidation of **1** with $HClO_4$, is rhombic and exhibits clearly resolved ^{195}Pt coupling in the high-field feature (^{195}Pt $I = 1/2$, 33.8%, 66.2% $I = 0$). Simulation of the spectrum[12] provided estimates of the spin Hamiltonian parameters (Fig. 3). Only the high-field Pt ($I = 0$) feature exhibits superhyperfine

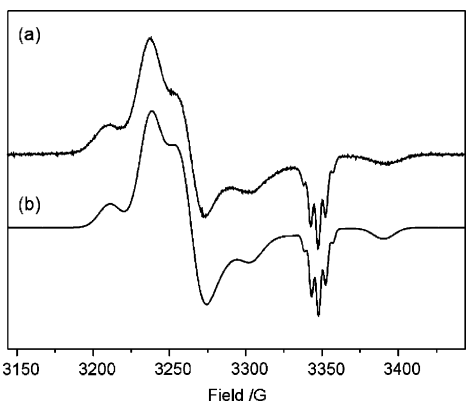

Fig. 3 (a) X-Band EPR frozen solution spectrum of $[Pt([9]aneS_3)_2]^{3+}$ at 77 K in $HClO_4$. (b) Simulated spectrum with $g_{xx} = 2.047$, $g_{yy} = 2.031$ and $g_{zz} = 1.980$; $|A_{xx}|(^{195}Pt) = 50$, $|A_{yy}|(^{195}Pt) = 3$ and $|A_{zz}|(^{195}Pt) = 80 \times 10^{-4}$ cm^{-1}; $|a_{xx}|(^{1}H) = 0.0$, $|a_{yy}|(^{1}H) = 0.0$ and $|a_{zz}|(^{1}H) = 4.3 \times 10^{-4}$ cm^{-1}. Gaussian linewidths: $W_{xx} = 45$, $W_{yy} = 48$ and $W_{zz} = 9$ MHz. A-Strain in the ^{195}Pt component: $AS_{xx} = 30$, $AS_{yy} = 30$ and $AS_{zz} = 60$ MHz. From our simulations and simulated line-widths we estimate errors of ±0.001 and $\pm 5 \times 10^{-4}$ cm^{-1} for the principal components of the *g*- and *A*-tensors, respectively.

coupling which was simulated by the inclusion of coupling [$a_{ii}(^1H)$] to four equivalent ^{1}H nuclei. We included A-strain (AS_{ii})[13] in the ^{195}Pt component in addition to the usual inhomogeneous line-broadening (W_{ii}, $i = x, y, z$) in our simulations. We were unable to determine the relative signs of the principal values of the ^{195}Pt hyperfine tensor because of the poor resolution of the fluid solution EPR spectrum of $[Pt([9]aneS_3)_2]^{3+}$ in $HClO_4$ (Fig. S4 in ESI†).

In order to interpret the EPR spectrum of $[Pt([9]aneS_3)_2]^{3+}$ we followed our approach developed for the related d^9 species $[Au([9]aneS_3)_2]^{2+}$.[10b] Thus, g_{xx} and g_{yy} are assigned to orientations lying in the equatorial PtS_4 plane, with g_{zz} perpendicular to this plane. Crystal field theory arguments place the unpaired electron in the Pt $5d_{z^2}$ orbital. DFT calculations are consistent with this interpretation, predicting that the dominant metal component of the SOMO is $5d_{z^2}$ (see below). In this case, the principal components of the *g* and *A*-matrices are given by eqn (1) and (2), respectively:[14]

$$\begin{aligned} g_{xx} &= g_e + 6\delta_{xy} \\ g_{yy} &= g_e + 6\delta_{xz} \\ g_{xx} &= g_e \end{aligned} \tag{1}$$

$$\begin{aligned} A_{xx} &= A_s + P_d\left[\frac{-2}{7}\alpha^2 + \Delta g_{xx} + \frac{1}{14}\Delta g_{yy}\right] \\ A_{yy} &= A_s + P_d\left[\frac{-2}{7}\alpha^2 + \Delta g_{yy} + \frac{1}{14}\Delta g_{xx}\right] \\ A_{zz} &= A_s + P_d\left[\frac{4}{7}\alpha^2 - \frac{1}{14}(\Delta g_{xx} + \Delta g_{yy})\right] \end{aligned} \tag{2}$$

where g_e is the free electron *g*-value, Δg_{ii} are the shifts in the *g*-values from g_e, P_d is the electron–nuclear dipolar coupling parameter for Pt 5d electrons, and α is the linear combination of atomic orbitals (LCAO) coefficient of the Pt $5d_{z^2}$ orbital in the SOMO. The δ_i terms are the weighted average ground state-excited state energy gaps:

$$\delta_i = \sum_{k \neq 0} \frac{\lambda c_{ik}^2}{E_0 - E_k}$$

where λ is the spin–orbit coupling constant for Pt 5d electrons, and c_{ik} is the LCAO coefficient of the *i*th atomic orbital in the *k*th molecular orbital. A_S is the isotropic Fermi contact term given by:

$$A_s = \langle A \rangle - P_d\left(\frac{\Delta g_{xx} + \Delta g_{yy} + \Delta g_{zz}}{3}\right) \tag{3}$$

We would expect g_{xx} and $g_{yy} > 2.0023$ and $g_{zz} = 2.0023$. Our simulated spectrum reveals a significant negative contribution to Δg_{zz} that may result from limitations of the first order treatment that neglects second order spin–orbit coupling and low energy LMCT in complexes containing heavy transition metal centres co-ordinated by thioether ligands.[10b] In addition, eqn (1) and (2) assume that the principal axes of the *g*- and *A*-matrices are coincident and we have assumed this to be the case experimentally because we achieve good simulations without including non-coincidence effects. However, it should be noted that this situation is not required for the

non-symmetric $[Pt([9]aneS_3)_2]^{3+}$ because all of the 5d orbitals can mix. This scrambling of d-orbital functions can give rise to *g*- and *A*-matrix non-coincidence effects.[10b] DFT calculations (see later) suggest that the dominant contribution to the SOMO is $5d_{z^2}$ (30.4%) and that there are negligible contributions from the other 5d orbitals. Thus, non-coincidence effects in $[Pt([9]aneS_3)_2]^{3+}$ are likely to be minor.

A combination of eqns (2) and (3) gives:

$$A_{zz} = \langle A \rangle + P_d \left[\frac{4}{7}\alpha^2 - \frac{\Delta g_{zz}}{3} - \frac{17}{14}(\Delta g_{xx} + \Delta g_{yy}) \right] \qquad (4)$$

We used a calculated value of $P_d = 590.4 \times 10^{-4}\ cm^{-1}$ for the Pt(III) with a d^7 configuration using Rieger's methodology[15] to derive estimates of α^2 from the spin Hamiltonian parameters derived from simulation using combinations of A_{ii} with differing signs in eqn (4). We obtained realistic estimates of α^2 of 0.25 and 0.24 by using $A_{xx} = +80$, $A_{yy} = -3$ and $A_{zz} = -50 \times 10^{-4}\ cm^{-1}$, and $A_{xx} = +80$, $A_{yy} = +3$ and $A_{zz} = -50 \times 10^{-4}\ cm^{-1}$, respectively. Thus, after including our estimated errors in the spin Hamiltonian parameters we place an upper limit on α^2 of 0.25 in the SOMO.

We have shown that ZORA SR DFT calculations employing all-electron TZP basis sets derived from the ZORA/TZP database of the ADF suite of programs can reproduce the principal features of the geometric and electron structures of $[Au([9]aneS_3)_2]^{2+}$ and $[Ag([18]aneS_6)_2]^{2+}$.[10b] The experimental and calculated structural parameters for the PtS_6 coordination sphere of a model of $[Pt([9]aneS_3)_2]^{3+}$ using this level of theory are compared in Tables S1 and S2 (see ESI†). For $[Pt([9]aneS_3)_2]^{3+}$, the calculations reveal axial and equatorial Pt–S distances that are 0.10 and 0.06 Å longer, respectively, than those in the experimentally determined structure of $[Pt([9]aneS_3)_2]^{3+}$ in **2**·MeCN and S–Pt–S bond angles that differ by *ca.* 2° from their counterparts in the experimental structure. The ability of the DFT calculations to reproduce the principal features of the geometry of $[Pt([9]aneS_3)_2]^{3+}$ and the experimental validation of the approach for $[Au([9]aneS_3)_2]^{2+}$,[10b] suggest that these DFT calculations are of sufficient quality to permit a qualitative understanding of the electronic properties of $[Pt([9]aneS_3)_2]^{3+}$. The calculations reveal a SOMO that is 30.4% Pt $5d_{z^2}$, 47.5% axial S 3p and 12.1% equatorial S 3p in character and identify four H-atoms, associated with the ligand backbone, which are the only protons that possess significant spin density (Fig. 4). The calculations indicate that these protons are those responsible for the superhyperfine coupling observed in the EPR spectrum of $[Pt([9]aneS_3)_2]^{3+}$ (Fig. 3).

In summary, we have prepared and structurally characterised **2**·MeCN as the first complex that contains a Pt(III) centre in a distorted octahedral S_6 geometry. EPR spectroscopy and DFT calculations show that $[Pt([9]aneS_3)_2]^{3+}$ possesses a Pt $5d_{z^2}$ ground state with significant axial S-character in the SOMO. These results demonstrate the versatility of thioether macrocycles as ligands to stabilise metal centres in highly unusual oxidation states.

We thank the EPSRC and the University of Nottingham for support and funding. MS gratefully acknowledges receipt of a Royal Society Wolfson Merit Award and of a Royal Society Leverhulme Trust Senior Research Fellowship. We also thank Johnson Matthey plc for loans of platinum metals.

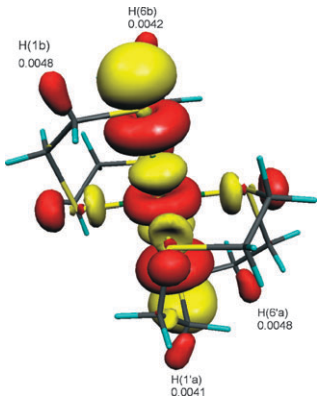

Fig. 4 Isosurface plot at 0.03 e $Å^{-3}$ of the α-spin SOMO of $[Pt([9]aneS_3)_2]^{3+}$ derived from a BP-TZP relativistic DFT calculation showing spin densities for the protons H(1b), H(6b), H(1′a) and H(6′a).

Notes and references

1 R. Usón, J. Forniés, L. R. Falvello, M. Tomás, J. M. Casas, F. A. Cotton and X. Feng, *J. Am. Chem. Soc.*, 1993, **115**, 4145–4154.
2 D. P. Bancroft, F. A. Cotton, L. R. Falvello and W. Schwotzer, *Inorg. Chem.*, 1986, **25**, 763–770.
3 D. P Bancroft and F. A. Cotton, *Inorg. Chem.*, 1988, **27**, 4022–4025.
4 R. Cini, F. P. Fanizzi, F. P. Intini and G. Natile, *J. Am. Chem. Soc.*, 1991, **113**, 7805–7806.
5 A. Alonso, J. M. Casas, F. A. Cotton, X. Feng, J. Forniés, C. Fortuño and M. Tomás, *Inorg. Chem.*, 1999, **38**, 5034–5040.
6 R. Usón, J. Forniés, M. Tomás and B. Menjón, *Organometallics*, 1986, **5**, 1576–1581.
7 H. Bois, N. G. Connelly, J. G. Crossley, J. C. Guillorit, G. R. Lewis, A. G. Orpen and P. Thornton, *J. Chem. Soc., Dalton Trans.*, 1998, 2833–2838.
8 X. M. Ren, H. Okudera, R. K. Kremer, Y. Song, C. He, Q. J. Meng and P. H. Wu, *Inorg. Chem.*, 2004, **43**, 2569–2576.
9 H. Alves, D. Simão, I. Cordeiro Santos, V. Gama, R. Teives Henriques, H. Novais and M. Almeida, *Eur. J. Inorg. Chem.*, 2004, 1318–1329.
10 (*a*) A. J. Blake, R. O. Gould, A. J. Holder, T. I. Hyde, A. J. Lavery, M. O. Odulate and M. Schröder, *J. Chem. Soc., Chem. Commun.*, 1987, 118–120; (*b*) J. L. Shaw, J. Wolowska, D. Collison, J. A. K. Howard, E. J. L. McInnes, J. McMaster, A. J. Blake, C. Wilson and M. Schröder, *J. Am. Chem. Soc.*, 2006, **128**, 13827–13839; (*c*) C. W. G. Ansell, G. J. Lewis, P. R. Raithby, J. N. Ramsden and M. Schröder, *J. Chem. Soc., Chem. Commun.*, 1982, 546–547; (*d*) A. J. Blake, R. O. Gould, T. I. Hyde and M. Schröder, *J. Chem. Soc., Chem. Commun.*, 1987, 431–433; (*e*) G. Reid, A. J. Blake, T. I. Hyde and M. Schröder, *J. Chem. Soc., Chem. Commun.*, 1988, 1397–1399; (*f*) A. J. Blake, A. J. Holder, T. I. Hyde and M. Schröder, *J. Chem. Soc., Chem. Commun.*, 1989, 1433–1434; (*g*) A. J. Blake, G. Reid and M. Schröder, *J. Chem. Soc., Dalton Trans.*, 1990, 3363–3373; (*h*) J. Lewis and M. Schröder, *J. Chem. Soc., Dalton Trans.*, 1982, 1085–1089.
11 M. Matsumoto, M. Itoh, S. Funahashi and H. D. Takagi, *Can. J. Chem.*, 1999, **77**, 1638–1647.
12 S. Stoll and A. Schweiger, *J. Magn. Reson.*, 2006, **178**, 42–55; S. Stoll and A. Schweiger, *Biol. Magn. Reson.*, 2007, **27**, 299–321.
13 F. E. Mabbs and D. Collison, *Electron Paramagnetic Resonance of d Transition Metal Compounds*, Elsevier, Amsterdam, 1992.
14 P. H. Rieger, *Coord. Chem. Rev.*, 1994, **135**, 203–286.
15 P. H. Rieger, *J. Magn. Reson.*, 1997, **124**, 140–146.